

Prospects for Improving the Intrinsic and Extrinsic Properties of Magnesium Diboride Superconducting Strands

E.W. Collings, M. D. Sumption, M. Bhatia* M. A. Susner, and S. D. Bohnenstiehl,

Laboratories for Applied Superconductivity and Magnetism,

Department of Materials Science Engineering, The Ohio State University

477 Watts Hall, 2041 College Rd, Columbus OH 43210

*Now at the Texas Accelerator Center, The Woodlands, TX 77381

Abstract

The magnetic and transport properties of MgB₂ films represent performance goals yet to be attained by powder-processed bulk samples and conductors. Carbon-doped films have exhibited upper critical fields, $\mu_0 H_{c2}$, as high as 60 T and a possible upper limit of more than twice this value has been predicted. Very high critical current densities, J_c , have also been measured in films, e.g. 25 MA/cm² in self field and 7 kA/cm² in 15 T. Such performance limits are still out of the reach of even the best MgB₂ magnet wire. In discussing the present status and prospects for improving the performance of powder-based wire we focus attention on (1) the *intrinsic* (intragrain) superconducting properties of MgB₂ -- H_{c2} and flux pinning, (2) factors that control the efficiency with which current is transported from grain-to-grain in the conductor, an *extrinsic* (intergrain) property. With regard to Item-(1), the role of dopants in H_{c2} enhancement is discussed and examples presented. On the other hand their roles in increasing J_c , both via H_{c2} enhancement as well as direct fluxoid/pining-center interaction, are discussed and a comprehensive survey of H_{c2} dopants and flux-pinning additives is presented. Dopant selection,

chemistry, methods of introduction (inclusion), and homogeneity of distribution (via the rounding of the superconducting electronic specific heat transition) are considered. Current transport through the powder-processed wire (an extrinsic property) is partially blocked by the inherent granularity of the material itself and the chemical or other properties of the intergrain surfaces. Overall porosity, including reduced density and intergranular blocking, is quantified in terms of the measured temperature dependence of the normal-state resistivity compared to that of a clean single crystal. Several experimental results are presented in terms of percent effective cross-sectional area for current transport. These and other such results indicate that in many cases less than 15% of the conductor's cross sectional area is able to carry transport current. It is pointed out that densification in association with the elimination of grain-boundary blocking phases would yield five-to ten-fold increases in J_c in relevant regimes, enabling the performance of MgB₂ in selected applications to compete with that of Nb₃Sn.

Keywords: MgB₂, Upper critical field, irreversibility field, transport J_c , connectivity

PACS: 74.25.Sv, 74.25.Sv, 74.70.Ad

Outline

1.0. Introduction

1.1. Intrinsic Properties

1.2. Extrinsic Properties- Connectivity and Porosity Issues

2.0. Intrinsic Properties of MgB₂ Conductors

2.1. Upper Critical Fields and Irreversibility Fields and their Enhancement by Dopant Induced Impurity Scattering

2.1.1. Theory

2.1.2. Selection of Dopants for H_{c2} Optimization

2.2. Critical Current Density and its Enhancement by Doping and Flux Pinning

2.2.1. Doping in General

2.2.2. Flux Pinning and Doping Mechanisms

2.3 Electronic Specific Heat and Compositional Inhomogeneity

3.0 Extrinsic Properties of Polycrystalline MgB₂

3.1. Porosity

3.2. General Connectivity

4.0 Discussion

4.1 Intrinsic Properties

4.1.1. Electronic Properties

4.1.2. Lattice and Related Properties

4.2 Extrinsic Properties

5.0 Conclusion

1.0. Introduction

The initial announcement of superconductivity below a T_c of about 40 K in MgB₂ by Akimitsu in 2001[1] triggered extensive research on its preparation in film, bulk, and wire forms as well as its electrical, magnetic, and mechanical properties. Already by June of that year more than 250 research papers had been published and by November 2001 MgB₂ was the subject of a comprehensive review by Buzea and Yamashita [2]. With upper critical fields, H_{c20} , no higher than about 18 T in single crystals, bulks, and wires, and with critical current densities, J_c , mostly less than about 10^4 A/cm² at 5 K, 5 T, MgB₂ tended to be of scientific rather than practical interest. But it was the report of very high H_{c2s} in alloyed (“dirty”) thin films, accompanied by promisingly high J_c s by Eom et al. in May 2001 [3], along with the subsequent reports of H_{c20s} of more than 70 T by Braccini et al [4] in 2005, that alerted the community to the possibility of wide-spread practical applications if such properties could be transferred to tapes and wires on a large scale. Subsequent years have seen the establishment of commercial companies dedicated to the manufacture of bulk MgB₂ objects and long lengths of MgB₂ tapes and wires. At the same time steady improvements in H_{c2} and J_c have been reported. As a result MgB₂ is on the threshold of widespread practical application, an important example being magnets for magnetic resonance imaging. But to take the next step, whether we are interested in high field 4 K operation, or in the more energy efficient 20 K temperatures regimes well out of the range of the present NbTi and Nb₃Sn wires, further improvement of the in-field J_c is needed. In addressing this issue we must recognize two classes of properties (what might be termed “intrinsic” and “extrinsic”, respectively) that are in urgent need of fundamental research. Below, we summarize some of the key issues that need to be addressed.

1.1. Intrinsic Properties

The essential intrinsic (i.e. intragranular) properties of polycrystalline MgB₂ are H_{c2} and flux pinning (or, alternatively, intra-grain J_c). Increases in the former are always welcome, but the already measured H_{c20S} of more than 33 T [5] are usefully high provided they are homogenous. That this is not yet the case is all too evident in experimental results to-date. We must also consider the anisotropy of the superconducting properties, as manifested particularly in the H_{c2} values for field along the basal planes as compared to those along the c -axis. This anisotropy can be addressed at an intrinsic level by dopant selection, as some dopants modify this intrinsic anisotropy. Anisotropy also has implications for grain-to-grain current flow in untextured polycrystalline materials, but this is better addressed as a kind of effective connectivity within the extrinsic group of properties.

Beyond this, there must be a satisfactorily high level of flux pinning. Such is not the case at present; flux pinning centers yielding high bulk pinning forces, F_p , with maxima located at fields much higher than the existing 4-5 T at 4 K (i.e., at about 20% of the irreversibility field, H_{irr}) are preferred. Extensive research has already been carried out on the effects of dopant additions on H_{c2} and J_c . Indeed, numerous metallic elements, borides, carbides, oxides, and even organic compounds have been added. This research needs to be continued on a rational scientific basis and redirected if MgB₂ is to operate successfully at higher fields and temperatures. Necessary to generate improved properties is the presence of suitably chosen *combinations* of dopants (elements in substitutional solid solution) plus nano-size flux pinning additions (e.g. [6]). However, as will be argued below, the two most crucial improvements needed to significantly enhance MgB₂ performance are: (i) homogenous dopant induced H_{c2} enhancement, and (ii) large increases in connectivity (the removal of inter-grain resistive boundaries).

Texturing (or anisotropy reduction) and flux pinning, while important, will not influence final transport J_c as strongly as those properties. While homogeneous doping and H_{c2} enhancement can be considered intrinsic properties, connectivity is an inherently extrinsic property.

1.2. Extrinsic Properties- Connectivity and Porosity Issues

In addition to intrinsic-property improvement substantial across-the-board increases in J_c will accompany increases in the superconductor-material's effective cross-sectional area for the conduction of transport current. The possibility of "cross-sectional deficiency" was first recognized by Rowell [7][8] who noted that the normal-state electrical resistivities of some polycrystalline thin film samples of MgB_2 could be as high as $500 \mu\Omega\text{cm}$ – well beyond the regime of metallic conductivity. Not only normal-current flow, but supercurrent flow is also expected to be reduced by this cross-sectional deficiency, removal of which is estimated to increase the J_c of a given polycrystalline sample by factors of five-to ten. Although clean grain boundaries as such do not impede supercurrent flow [9], the observed intergranular partial coatings of insulating MgO or amorphous BO_x [10] will certainly do so. Formation of the coating, an interesting problem in solid state chemistry, is an area of active study. Research is focussing on the possibility of reducing or eliminating it [11] leading to improved intergranular connectivity.

Magnesium diboride wires are made by powder-in-tube processes, either *ex-situ* in which ready-made MgB_2 powder is packed into a tubular jacket and drawn down or *in-situ* in which the jacketed elemental Mg and B ingredients are reacted together at final wire size. Although the *ex-situ* wire is subject to the porosity expected of any powder-processed body, the *in-situ* wire filling is made even more porous by the voids remaining from the prior Mg particles after the

Mg+2B→MgB₂ reaction. Various consolidation techniques are beginning to be introduced in attempts to reduce porosity in bulk samples and wires. Different reaction routes to MgB₂ formation that will lead directly to reduced porosity are also being studied [12].

2.0. Intrinsic Properties of MgB₂ Conductors

The very high H_{c2} s reported for dirty films ([3] and subsequently [4]) which alerted the community to the possibility of high field and other practical applications, continue to serve as useful references against which the H_{c2} s of evolving MgB₂ conductors can be compared. Likewise the high J_c s of dirty films can be seen as goals, bearing in mind that although films are not immune to connectivity problems, at least they are not porous.

2.1. Upper Critical Fields and Irreversibility Fields and their Enhancement by Dopant-Induced Impurity Scattering

2.1.1. Theory: For dirty, non-paramagnetically limited, single-band, low-temperature superconductors the following well known expression for zero-K upper critical field, H_{c20} can be obtained by starting with Maki's dirty-limit H_{c20} and inserting an expression for the BCS zero-K thermodynamic critical field, H_{c0} , thus:

$$\rho_0 = \frac{3.27 \times 10^{-5}}{\gamma} \left(\frac{H_{c20}}{T_c} \right) = \frac{2.23 \times 10^{-5}}{\gamma} \left(\frac{-dH_{c2}}{dT} \right)_{T_c} \quad (1)$$

where ρ_0 is the impurity resistivity and γ the electronic specific heat coefficient. Equation (1) indicates that the value of $H_{c2}(T)$ at 0 K and its slope at T_c are proportional to ρ_0 (alternatively, inversely proportional to the charge-carrier diffusivity, where $1/\rho_0 = e^2 N_F D$). Increases in H_{c20} would be expected to follow directly from the introduction of charge-carrier-scattering impurities into the superconductor's lattice structure - a rule that has guided the design of low temperature

superconductors over the years. But this simple rule is no longer obeyed for MgB₂, for which there is no direct relationship between H_{c20} and ρ_0 [13].

In the compound MgB₂ the presence of Mg stabilizes the B sub-lattice in the form a honeycomb-like stack of hexagonal networks, essentially a new allotrope of B. The B honeycomb dominates the electronic structure which can be thought of as deriving from σ bonding within the B plane (leading to a “ σ band”) and π bonding both in and out of the plane (leading to a “ π band”) [14]. The bands have their individual Fermi densities-of-state, superconductive energy gaps, and scattering relation times, D_σ and D_π , respectively [15].

With reference to a copious body of experimental upper critical field results comparable to that of Figure 1, Gurevich et al [16][17] [18] have been able to illustrate and explain MgB₂'s unusual critical-field temperature dependence in terms of the electronic diffusivities (D_π and D_σ) associated with its two-band conductivity:

$$\sigma = e^2 (N_{F\pi} D_\pi + N_{F\sigma} D_\sigma) \quad (2)$$

The introduction of two diffusivities results in pronounced departures from the single-band predictions; in particular, $H_{c2nearTc}$, and H_{c20} respond individually to D_π and D_σ . Thus, according to Gurevich et al [16] and to a first approximation:

$$H_{c2nearTc} \propto \frac{1}{\lambda_1 D_\sigma + \lambda_2 D_\pi} \quad (3)$$

(in which the λ s are appropriate functions of the intraband and interband electron-phonon coupling constants [16], see also Section 4.1.2) and

$$H_{c20} \propto \frac{1}{\sqrt{D_\sigma D_\pi}} \quad (4)$$

Simply stated, near the critical temperature $H_{c2nearTc}$ varies inversely as the weighted arithmetic mean of D_σ and D_π while $H_{c2near0K}$ (H_{c20}) varies inversely as their geometric mean. Thus while increasing impurity scattering is beneficial to H_{c2} over the entire temperature range for both single-band and double-band superconductors, in the latter case (and recognizing the independence of D_π and D_σ) it allows H_{c20} to diverge to very large values in response to decreases in either D_σ or D_π .

H_{c2} at “High Temperatures”: Suppose, as has turned out to be the case for dirty MgB₂ films, $D_\pi \ll D_\sigma$ (i.e., π scattering much stronger than σ scattering) Equation (3) approximates to

$$H_{c2nearTc} \propto \frac{1}{\lambda_1 D_\sigma} \quad (5)$$

$H_{c2nearTc}$, which is in general controlled by the **greater** of the two diffusivities, is in this case controlled by D_σ . Further changes in $H_{c2nearTc}$ would be expected to follow a manipulation of D_σ .

H_{c2} at “Low Temperatures”: Referring to Equation (4) in which D_σ and D_π are tied together as a product (even though D_π is the “dominant” component), it would seem that manipulation of either of them would influence H_{c20} . But examination of the H_{c20} relationship in more detail reveals that for very different diffusivities

$$H_{c20} \propto \frac{1}{D_\sigma} \quad D_\sigma \ll D_\pi \quad (6)$$

$$H_{c20} \propto \frac{1}{D_\pi} \quad D_\pi \ll D_\sigma \quad (7)$$

so the H_{c20} is controlled by the smaller of the two diffusivities – e.g., the D_π in dirty MgB₂ films. As pointed out by Gurevich [18] H_{c20} s close to the BCS paramagnetic limit of $H_p = 65$ T (see Figure 1 [19]) are already being attained in MgB₂. Furthermore, given that BCS underestimates

H_p by the factor $(1+\lambda)$ where λ is some global electron-phonon coupling constant, values as high as 130 T may in principal be achievable. Based on the spectacular thin film results Gurevich et al. [16] pointed out that the use of MgB₂ will open a “new domain of application for superconducting magnets”, one that is outside the reach of NbTi and to some extent Nb₃Sn, implying that in general enhancements to the H_{c2} will follow the judicious introduction of scattering impurities.

2.1.2. Selection of Dopants for H_{c2} Optimization: It has been suggested that: (i) macroscopic particles that contribute to lattice distortion enhance both π and σ scattering, (ii) disorder on the Mg sublattice (e.g. by Al addition) can increase the π scattering, (iii) oxygen when substituting for B was expected to provide strong σ scattering; so also was C [16]. By now a multitude of papers have described the benefits of adding C in one form or another to the MgB₂ lattice. Carbon has been added in elemental form (microspheres, nanotubes, nanodiamond) or by way of C-containing compounds such as SiC, TiC, B₄C, organic compounds, and so on (see below). The work has been largely semi-empirical in nature albeit related to and guided by the principles outlined above.

Although C when doped into the B lattice might be expected to increase σ scattering (as predicted by recent electronic-structure calculations [20]), Angst et al [21] and more recently Gurevich [18] have offered experimental evidence in support of a π -scattering mechanism. These authors agree that the upward curvature of the low-temperature $H_{c,field\ parallel}$, or at least its lack of negative curvature, see Figure 1, points to the dominance of π -band scattering. Although dopant induced buckling of the a - b (Mg) planes has been suggested as a mechanism for the enhanced π

scattering [18][21] the latter authors have concluded that it is in fact an intrinsic result of C substitution but for reasons that are not fully understood [18][21].

In selecting dopants, reaction chemistry is an important consideration. The success of SiC as a dopant for C [22] relies on the fact that, during in-situ processing, the Mg decomposes SiC and releases atomic C before the onset of the $\text{Mg}+2\text{B}\rightarrow\text{MgB}_2$ reaction. This is clearly demonstrated in the results of differential scanning calorimetry (DSC), Figure 2. All DSC data depicted there were collected with a TA Instruments DSC2920 under argon flow, using an Fe pan. Three different runs were made: (1) The first with Mg only (solid line) exhibits the endothermic peak associated with Mg melting at about 650°C. (2) A run made just with mixed SiC and Mg powders (the dashed line) evinces the reduction of SiC by Mg at 524°C again followed by Mg melting at 650°C. (3) The third curve (dash-dot) shows the response of a sample of mixed Mg and amorphous B (99+% pure) powders. It depicts the endothermic surface reaction described in [23] as well as the onset of MgB_2 formation at 615°C below the Mg's 650°C melting point [23].

Since dopant concentrations are generally small, attention must be given to ensuring that they are uniformly distributed and/or incorporated into the lattice. Thinking along these lines, Ribiero et al [24] selected B_4C as a source of C doping reckoning that the C and the B were already mixed on an atomic-length scale. A similar strategy, and other considerations, also guided the selection of the diborides TiB_2 , ZrB_2 , and NbB_2 as potential H_{c2} -enhancing dopants [5]. Of these, ZrB_2 was the most potent, and with an $H_{c2,4K}$ of 29 T, became the subject of more detailed study [25], Figure 3. Two bulk samples were made, the first with binary stoichiometric MgB_2 and the second with 7.5 mol% ZrB_2 addition. They were prepared by the in-situ reaction of a stoichiometric mixture of 99.9% pure Mg and amorphous B (99+%) powders after SPEX

milling and compacting into pellets. Critical field measurements were performed resistively at 4 K, and magnetically at higher temperatures [25]. In Figure 3, the filled triangles give the H_{irr} vs T for binary MgB_2 , the filled circles give the response of the ZrB_2 -doped sample, and the open triangles represent the percentage increase in H_{irr} resulting from that doping. Based on XRD measurements, which showed increases in both the c - and a -lattice parameters, we deduced that Zr was substituting on the Mg site. Thus, we might expect the dopant to be effective primarily at lower temperatures (assuming π band scattering). It is interesting to note that the increase for ZrB_2 [25] is not very different from that contributed by SiC doping [22]. Additionally, even with substitutional doping the possibility of unreacted residues cannot be ignored. Although they were not present as a result of ZrB_2 doping, they were observed with NbB_2 doping [25] and are known to be present after SiC doping [22].

Of course, the unreacted residue is not necessarily inert, and may contribute flux pinning centers, or indirectly increase either π and σ scattering via lattice distortion and in that way increase H_{irr} . However, although numerous dopants (including metallic elements, borides, carbides, oxides, and organic compounds) have been added to MgB_2 little direct attention has been paid to the possible existences of such dual doping mechanisms.

2.2. Critical Current Density and its Enhancement by Doping and Flux Pinning

2.2.1. Doping in General: In considering the J_c s attainable in MgB_2 bulk samples we turn again, as a first basis of comparison, to the results of thin films measurements, with reference to the work of Eom et al [3] and many subsequent researchers. Figure 4 displays the J_c s of MgB_2 films made by various techniques -- e-beam evaporation, thermal co-evaporation, hybrid physical-chemical vapor deposition, and pulsed-laser deposition (PLD). There are two versions

of PLD – “in-situ” in which the MgB₂ is directly deposited and “ex-situ” in which a PLD-deposited B layer is exposed to Mg vapor, although in practice, some post-deposition of Mg seems to be needed even in the “in-situ” case.

These thin-film “reference J_c s” are compared to those of commercially processed binary MgB₂ powder-in-tube (PIT) wires of varying filament counts in Figure 5. These strands were all made via the in-situ route by Hyper Tech Inc. from mixed Mg powder (10% excess Mg) and 99% pure amorphous B powder. They typically achieved 4 K J_c s of 10^5 A/cm² at 4.5-5 T, and 10^4 A/cm² at 8 T, about an order of magnitude below the best thin film data. We go on to show some incremental improvements in J_c that result from: (i) the introduction of even more Mg and (ii) the doping of the excess-Mg strand with SiC particles, Figure 6. For this sample set the best results (10^5 A/cm² and 10^4 A/cm² at 6 T and 11.5 T, respectively) are found when the excess-Mg level is raised to 15% and SiC is added. Still further improvements are depicted in Figure 7 which emphasizes the effectiveness of the C-containing dopants e.g. maleic anhydride, SiC, and C itself when appropriately introduced. On the best of such samples the 10^4 A/cm² J_c is obtained at a field as high as 13 T. Although this result could be said to be about a factor of three off from the best thin film data reported at these fields, there is in fact a paucity of data in this regime, some of the higher performing films having been measured only at lower fields.

Over the years some 40-odd dopant species have been introduced into MgB₂, Table 1. It is possible to discern a few guiding principles that may have governed their selection. The inclusion of the metallic elements and metal oxides were clearly attempts to introduce normal flux-pinning centers. The borides, nitrides and C-containing dopants were added to increase H_{c2} and hence to increase the effectiveness of already present pinning centers as described below. Some additions

likely played a dual role – decomposing to partially substitute into the MgB₂ lattice while leaving a flux-pinning particulate residue.

In concluding this section on J_c enhancement it is important to note that: (i) The primary purpose of a few of the compositional modifications and/or dopant additions (e.g., CaC₆) is to reduce grain-boundary contamination and improve connectivity, the subject Section 3 of this paper. (ii) Although useful as interim goals, the thin-film J_{cs} of Figures 4-7 are not the ultimate “gold standards”; essential to the Rowell connectivity analysis [7][8] was the fact that even polycrystalline films are subject to intergrain transport degradation. Even so, it is important to make and then measure films out to high fields at 4 K to explore the potential of MgB₂ in this field regime.

2.2.2. Flux Pinning and Doping Mechanisms: Apart from pure single crystals all MgB₂ samples – films, bulks, and wires – are polycrystalline in the as-prepared state and hence tend to be moderately well grain-boundary pinned. The introduction of dopants can have one or more effects which may combine to increase the bulk pinning strength: (1) by increasing the crystal’s H_{c2} and H_{irr} ; (2) by forming a wide distribution of point pinning centers each described by an elementary pinning force f_p ; (3) by producing localized lattice strains which also contribute to flux pinning. The magnitude and behaviour of J_c in an applied field H is described by a bulk pinning function, F_p , which represents an appropriate **summation** of the elementary pinning forces, f_p [92-94]. Summation leads to expressions for the bulk pinning force density originally written in the form:

$$F_p = H_{c2}^m f(h) \quad \text{where } h = H/H_{c2} \quad (8)$$

Recognizing that for MgB₂ with an H_{irr} (the actual field at which F_p vanishes) that is significantly less than H_{c2} we need to define $h = H/H_{irr}$. Although part of the prefactor in the

expression for F_p derives from the field-normalization step, it is significant that another component comes from a condensation energy. Its presence indicates that dopants added to increase H_{c2} , although not pinning centers themselves, serve to increase the measured F_p of already-pinned samples.

The bulk pinning force field dependence, which generally rises to a maximum at some $h = h_{max}$, may be expressed in normalized form $F_p(h)/F_p(h_{max})$. This, for a given type of pinning center, is independent of temperature, a property known as **scaling**. The quotient $F_p/F_{p,max}$ is of the general form

$$f(h) \propto h^p(1-h)^q \quad (9)$$

As pointed out by Dew-Hughes [92] various classes or types of pinning by “normal” (non-superconducting) objects can be distinguished by the values assigned to the index p (with $q = 2$ for all normal pins), thus

$$\begin{aligned} h^0(1-h)^2 &\rightarrow \text{normal volume pinning} & d < a,b,c \\ h^{1/2}(1-h)^2 &\rightarrow \text{normal surface (grain boundary) pinning} & d < a,b \\ h^1(1-h)^2 &\rightarrow \text{normal point pinning} & d > a,b,c \end{aligned}$$

where a , b , c , characterize the dimensions of the pin and d is the fluxoid spacing; $d^2 = 1.15(\phi_0/B)$. Normal surface and point pinning can also be distinguished in terms of the corresponding values of h_{max} , viz. 0.2 and 0.33, respectively. Examples of the above normal pinning functions together with pinning-force data for a SiC-doped MgB_2 sample are given in Figure 8. This figure displays pronounced departures from scaling. The generally expected characteristic of grain-boundary pinning is seen for temperatures between 10-20 K. In the 20-30 K range, it appears that point pinning is beginning to dominate. At 20 K, we seem to have an intermediate case. Our normalizing field, H_{irr} , was based on a 100 A/cm^2 transport criterion. The lack of fit to the

curves at higher temperatures can be expected from a distribution of H_{irr} values (and underlying H_{c2} values) resulting from sample inhomogeneity. Evidence for this can be seen in the strong sensitivity of H_{irr} to measurement criteria, as well as in the heat capacity behaviour discussed below.

We have been referring above to normal pins -- i.e. non-superconducting pinning particles or regimes. Objects with κ -values differing markedly from the matrix pin by the so-called “ $\Delta\kappa$ ” mechanism which, according to Dew-Hughes [92] is characterized by a q -index of 1. Based on this criterion, none of the centers we have encountered in MgB_2 have exhibited $\Delta\kappa$ pinning.

2.3 Electronic Specific Heat and Compositional Inhomogeneity

In selecting and introducing potential H_{c2} - enhancing dopants it is important to be alert to the likelihood of compositional inhomogeneity in the resulting doped sample. In adding small fractions of dopant to a sample it is difficult to guarantee that the starting particles are uniformly dispersed. Even if they are, during reaction heat treatment the existence of finite diffusion distances will essentially guarantee a certain levels of inhomogeneity. Such will manifest themselves in terms of deviations from expected pinning curves -- difficult to de-convolute and separate from the effects of mixed pinning centers. However, analysis of the electronic specific heat jump of a superconducting material in the vicinity of its T_c can provide a sensitive quantitative measure of its degree of compositional homogeneity. The total low temperature specific heat of a metal (C_p) is the sum of a lattice (phononic) component, C_l , given by:

$$C_l = 9Nk \left(\frac{T}{\Theta_D} \right)^3 \int_0^{\Theta_D/T} \frac{x^4 e^x}{(e^x - 1)^2} dx \quad (10)$$

in which N = Avogadro's number, k = Boltzmann's constant (hence $Nk = 8.31$ J/mole.K) and an electronic component, C_e , given by γT for a normal metal and $\gamma[T_c .a.exp(-b/T)]$ for a superconductor below its transition temperature where a and b are metal-specific constants. At temperatures around the T_c of MgB_2 C_e is negligible compared to C_l (cf. Figures 9(a) and (b)). This has two consequences: (1) The specific heat data can be fitted to Equation (10) enabling a calorimetric- θ_D to be extracted. (2) A special technique must be invoked to expose the electronic component. On the assumption that the latter is magnetic field independent the superconductive C_e and its jump at T_c can be revealed and expanded after the in-field-measured specific heat is subtracted from the zero-field data. For this purpose a PPMS machine was used to take measurements in a magnetic field of 9 T over the temperature range 20-40 K. Figure 9(a) shows the results of C_p measurements on bulk samples of (i) binary stoichiometric MgB_2 , (ii) MgB_2 doped with 10% SiC (200 nm powder size), (iii) MgB_2 doped with 7.5% TiB_2 (<44 μm before milling) prepared as described in [5]. The curves, are similar in appearance, responding primarily to differences in Debye temperatures (see below) and with C_e jumps at T_c unresolved on the scale of the measurement. Figure 9(b), provides a detailed view of the electronic specific heat and its transition at T_c . A close look at the data reveals onset temperatures that decrease roughly in the sequence 38 K (MB700), 36.5 K (MBTi800), 35.5 K (MBSiC700) in agreement with the magnetically measured onsets [5] and in accord the results of Wälti et al who recorded a T_c of 37.5 K in their compacted pellet. Decreases in T_c below the nominal value of ~ 39 K are attributed to the presence of impurities [95,96] and in our case to the presence of dopants. The breadths of the superconducting jumps in Figure 9(b) contain information about the distribution of transition temperatures. No attempt is made here to fit the data to such a distribution although

it is possible to do so using standard techniques [97-99], nevertheless the presence of compositional inhomogeneities in the heavily doped MBTi700 and MBSiC700 is at least revealed qualitatively in the figure.

3.0. Extrinsic Properties of Polycrystalline MgB₂

3.1. Porosity

Randomly packed similar spheres will occupy space to a volume density of about 65% (although spheres of mixed sizes will fill the space more efficiently) for which reason compacted-powder pellets and the cores of PIT wires are inherently porous, e.g. Figure 10. Thus the packing densities of ex-situ-processed bulks and wires, based geometrically on the packing densities of powders, will be around 65%. Those of in-situ-processed bulks and wires are complicated by shrinkage associated with the $\text{Mg}+2\text{B}\rightarrow\text{MgB}_2$ reaction, but can be estimated using the data from Table 2. Our limiting estimates are based on two model scenarios.

Model-(1): *One mole of MgB₂ produced in-situ within a fixed-volume enclosure from a mixture of equi-sized Mg and B particles packed to a volume density-factor P_i .*

From Table 2 the volume ratio [Final (MgB₂)/Initial (Mg+2B)] = 17.2/23.0 = 0.75. It follows that if the initial packing density is P_i then the final density is $P_{f1} = 0.75P_i$. For example an initial mixed-powder close-packing of 65% leads to an MgB₂ powder density of 49%.

Model-(2): *One mole of MgB₂ produced in-situ within a fixed-volume enclosure from coarse Mg particles imbedded in fine B powder itself packed to a volume density-factor P_i – a kind of “micro-infiltration method” [100] more closely resembling reality.*

From Table 2, 13.74 cm^3 of Mg is required to produce 1 mol ($= 17.21 \text{ cm}^3$) of MgB_2 . The Mg pieces are imbedded in $9.25/P_i \text{ cm}^3$ of fine B powder (as in the Giunchi method, e.g. [100], but on a smaller scale). The overall packing density after reaction is therefore $P_{f2} = 17.21/[13.74+(9.25/P_i)]$. In this case, for example, a 65% dense B-powder environment would lead to an overall MgB_2 powder density of 62%. Taken together, these results as depicted in Figure 11 indicate that conventionally in-situ-processed bulks and PIT wires can be expected have packing densities in the range of 50-60% depending on the relative sizes of the Mg and B particles or powders.

Porosity impedes current flow and prevents the J_c of the MgB_2 body from attaining its intrinsic intragranular value. Furthermore, transport current flow is impeded by intergranular partial coatings, e.g. insulating MgO or amorphous BO_x [10]. The combined impact of porosity and current-blocking phases, illustrated in Figure 12, is to reduce the conductor's effective cross-sectional area for current flow by the inverse of F , the "Rowell factor" ($1/F$ is less than 1)..

The possibility of "cross-sectional deficiency" was first recognized by Rowell [7][8] who noted that the normal-state electrical resistivities of some polycrystalline thin film samples of MgB_2 could be as high as $500 \mu\Omega\text{cm}$ – well beyond the regime of metallic conductivity. Supercurrent flow is also expected to respond to this same cross-sectional deficiency, which causes the measured extrinsic J_c of a polycrystalline sample to be very much less than its intrinsic value.

3.2. General Connectivity

Since the effect of general porosity can be regarded as a geometrical phenomenon it is postulated that normal-state resistivity can be used as a measure of effective cross-sectional area

for transport in both the normal and superconducting states. Our connectivity analysis, which uses a modification of the Rowell approach [7,8], requires a detailed resistivity temperature dependence measurement but in response yields some additional information relevant to the sample's superconducting properties. We begin with an expression for the measured total resistivity:

$$\rho_m(T) = \rho_{0,m} + \rho_{i,m}(T) = F[\rho_0 + \rho_i(T)] \quad (10)$$

in which $\rho_{0,m}$ is the measured residual resistivity and $\rho_{i,m}(T)$ is the measured ideal (phononic) component. Finally, on the right-hand-side the terms within the brackets, ρ_0 and $\rho_i(T)$, are the intragrain residual- and ideal (phononic) resistivities, respectively, and the prefactor, $F > 1$, represents the observed resistivity enhancement due to the reduced effective transport cross-sectional area. Our approach consists in replacing the previously assumed universal $\rho_i(T)$ with the Bloch-Grüneisen function, thus:

$$\rho_m(T) = F \left[\rho_0 + \frac{k}{\theta_D} \left(\frac{T}{\theta_D} \right)^5 \int_0^{\theta_D/T} \frac{e^z z^5 dz}{(e^z - 1)^2} \right] \quad (11)$$

in which θ_D is the Debye temperature and k is a “materials constant” which we evaluate by fitting Equation (11) to a published set of single crystal data for which $F \equiv 1$. Fits of Equation (11) to the measured resistivity data then yield the following information: (1) the F -factor (and hence the percent connectivity, $100/F$) which enables the true intragrain J_c to be determined from the results of an accompanying J_c measurement; (2) the intragrain residual resistivity, ρ_0 ; (3) a resistive Debye temperature, θ_R , available for comparison to its calorimetrically measured counterpart, θ_D , see below.

By way of example we draw on the results of resistivity measurement on three pellets measured above for heat capacity; one binary stoichiometric sample, one doped with 7.5 % TiB₂,

and another doped with 10 % SiC. The results shown in Figure 13 after fitting to Equation (11) yielded the values of ρ_0 , θ_R , F , and percent connectivity ($100/F$) that are listed in Table 3.

Connectivity is the most practically significant result of the resistivity experiment. In Table 3 we note that the connectivities of the polycrystalline grains of the unalloyed and doped MgB₂ pellets vary from 11 to 23%. If these materials are representative of PIT wire cores, as no doubt they are, we can expect substantial increases in J_c e.g. (by factors of 9.1 and 4.3, respectively) beyond the values presented in Figure 7 in response to increases in connectivity.

4.0 Discussion

The potential “reach” of MgB₂ is subject to: (i) The optimization of H_{c2} and J_c through selected dopant additions, and (ii) increasing connectivity and minimizing porosity.

4.1 Intrinsic Properties

4.1.1. Electronic properties: Measurements on doped (“dirty”) thin films at liquid He temperatures have demonstrated the attainment of H_{c20s} approaching the BCS paramagnetic limit of $H_p = 65$ T (e.g. [18][19]. Furthermore, given that BCS underestimates H_p by the factor $(1+\lambda)$, values as high as 130 T may in principal be achievable [18]. The spectacular thin-film results have inspired researchers to seek equally high H_{c20s} in bulk pellets and wires, to achieve which suitable dopants need to be found and suitably dispersed. Likewise the high J_c s encountered in some thin film samples have provided goals for J_c development in wires. Progress has been reported in recent years such that, through the use of carefully selected dopants, wire J_c s are already on the threshold of the film values. Dopant selection is critical; they should have at least the following properties: (i) They should be able to be uniformly dispersed at an appropriate size

scale. (ii) If unreactive with MgB₂ or its precursors, their distribution should be such that they ideally interact with the coherence length of MgB₂. (iii) If the dopants react with MgB₂ or its precursors their products should either modify the Fermi surface of MgB₂ so that the critical fields are increased or the reaction products should follow the criteria established in (i). Table 1 summarizes a survey of the several classes of dopants that have been added to the binary base. Of them C, the only element that has so far been substituted for B, has turned out to be the most potent. Although it has been introduced in many forms – elemental C, C-containing inorganic and organic compounds, the most effective medium has been SiC, which is decomposed into Si+C by Mg prior to the Mg+2B→MgB₂ reaction. Carbon, which produces strong impurity scattering (hence high normal-state resistivity) in the π band (as well as the σ band) -- cf. Equation (7) -- is responsible for the upturn in H_{c2} at low temperatures [18]. It is important to note that whereas in dirty MgB₂ below T_c both the σ - and π -bands support superconductivity (mediated by the electron-phonon coupling constants $\lambda_{\sigma\sigma}$, $\lambda_{\pi\pi}$, $\lambda_{\sigma\pi}$, and $\lambda_{\pi\sigma}$) above T_c strong impurity scattering in the π -bands shunts normal transport current into the σ -band [101].

4.1.2. Lattice and Related Properties: Although the σ - and π -bands play different roles above and below T_c this difference does not invalidate the use of normal-state resistivity as a measure of superconducting state connectivity. Thus the B-G-based resistivity analysis has provided an effective cross-sectional area for general current transport as a measure of connectivity ($1/F < 1$). As well as quantifying the connectivity of powder-formed MgB₂ superconductors the B-G-based resistivity analysis yielded values for the *intragrain* residual resistivity, ρ_0 (not just its F -enhanced value). The increase in ρ_0 that accompanied the substitution of SiC (hence C) into MgB₂ (Table 3) indicates increased scattering in the σ -band, the primary conveyer of normal-

state current, in agreement with the results of thermal transport measurements on C-doped MgB₂ [102]. Deduced from the results of magnetic measurements [18, 21] (but not observed resistively for the above reason) C-doping also enhances scattering in the π -band and hence elevates the low temperature H_{c2} following Equation (7). Thus C doping enhances scattering in both the σ and the π bands, for which reason the observed increase in ρ_0 from 11.3 to 38.6 $\mu\Omega\text{cm}$ is *indirectly* related to a corresponding increase in $H_{c,4.2K}$ of from 21 to more than 33 T [5].

The B-G analysis also yields resistive Debye temperatures, θ_R . For our three bulk samples, both undoped and doped (average value 680 K), the values obtained are significantly lower than the deduced θ_{RS} of a pair several dense samples ($\theta_{av.} \sim 850$ K) and a single crystal (950 K). From this we deduce that in the present set of samples granularity and porosity disturb the phonon spectrum more strongly than sample chemistry. To confirm the resistively measured θ_R values the lattice specific heats of MB700, MBTi800, and MBSiC700 were measured at temperatures up to 300 K. The results (Figure 9(a)) were in satisfactory agreement with published data including those of Wälti et al. [95] who, in a paper dedicated to the specific heat of MgB₂, reported a value of 34 J/mole.K at 200 K, cf. 37.9 J/mole.K from Figure 9(a). The PPMS machine's internal software fitted the collected data to a standard Debye function and provided values of the calorimetric Debye temperatures, θ_D . By so doing it ignored the electronic component of total specific heat which, however, contributed less than about 2% to the lattice specific heat at 300 K. The values of θ_D so obtained, averaging ~ 670 K, agreed rather well with the resistive results. Wälti et al obtained a θ_D of 750 K on a pressed and sintered pellet of ex-situ MgB₂ powder heat treated for 72 h at 500°C, and Bud'ko et al [96] obtained 750 \pm 30 K on a pellet prepared in-situ for 2 h at 950°C. It is likely that these differences in θ_D respond to the differences in sample preparation conditions.

Given a measured T_c , e.g. from the electronic specific heat transition depicted in Figure 9b and either the measured transport- or calorimetric Debye temperature, θ_R or θ_D , an electron-phonon coupling constant, λ , can be directly obtained via the following modified version of the McMillan expression [103,104]

$$T_c = \frac{\theta_D}{1.45} \exp \left[\frac{-1.04(1 + \lambda)}{(\lambda - \mu^*(1 + 0.62\lambda))} \right] \quad (13)$$

In selecting a value for μ^* , the Coulomb repulsion parameter or “pseudopotential”, a survey of the literature ([105-112], but see in particular [111]) yielded $\mu^* = 0.10 \pm 0.02$ (actually equal to the 0.1 estimated for most metals [111]). Presented in Table 4, the results of our analysis provided $\lambda = 0.98$ for the sintered binary pellet and 0.89 and 1.02 for the doped ones. The value for our binary MgB₂ lies within the range of reported values [101][105-110][112-114], viz. 0.84 ± 0.21 .

What emerges from the specific heat experiment is a global average coupling parameter, λ , which according to [115] is related to the intraband and interband components, $\lambda_{\sigma\sigma}$, $\lambda_{\pi\pi}$, $\lambda_{\sigma\pi}$ and $\lambda_{\pi\sigma}$, by:

$$\lambda = \left\{ \frac{\lambda_{\sigma\sigma} + \lambda_{\pi\pi}}{2} \right\} + \sqrt{\left\{ \frac{\lambda_{\sigma\sigma} - \lambda_{\pi\pi}}{2} \right\}^2 + \lambda_{\sigma\pi} \lambda_{\pi\sigma}} \quad (14)$$

It is widely recognized (e.g. [106][113]) that electron coupling to the so-called E_{2g} phonon mode that represents in-plane B-B bond-stretching oscillations (hence $\lambda_{\sigma\sigma}$) is the dominant mechanism of superconductivity in MgB₂. Taken at face value Equation (14) indicates that the non-vanishing of interband coupling permits λ to be a function of both $\lambda_{\sigma\sigma}$ and $\lambda_{\pi\pi}$. as expected since the σ and π bands contribute to the superconductivity. Values for the individual λ components (both transport-related and superconductivity-related) have been tabulated by Mazin et al. [101]

according to whom the superconductive components are: $\lambda_{\sigma\sigma} = 1.02$, $\lambda_{\pi\pi} = 0.45$, $\lambda_{\sigma\pi} = 0.21$ and $\lambda_{\pi\sigma} = 0.15$. Inserting these values into Equation (14) yields a $\langle\lambda\rangle$ of 1.07 which is very close to $\lambda_{\sigma\sigma}$ itself (cf. our measured 0.98, Table 4) emphasizing the dominance of the in-plane coupling.

4.2 Extrinsic Properties

In general, current transport in all kinds of polycrystalline MgB₂ samples tends to be partially blocked by pores and grain-boundary precipitates such that the effective transport cross-sectional area is less than the conductor's geometrical cross-sectional area by a large factor, $F > 1$. Based on the assumption that both superconductive- and normal-state electrical current transport are moderated by the same effective cross-sectional area the result of a normal-state electrical resistivity temperature-dependence, $\rho_m(T)$, measurement can be manipulated so as to provide a value for F ; or what is the same thing, a “percent connectivity” $100/F$. This quantity is important to the development of practical MgB₂ conductors since it leads to estimates of the projected J_c s of microstructurally optimized materials quite apart from any improvements that might be expected to accompany the introduction of H_{c2} -enhancing and flux-pinning dopants. In Rowell's seminal articles on the subject [7,8], F -values for fairly clean MgB₂ were derived on the assumption of a universal ideal resistivity $\rho_i(T)$ for all samples.

We have confirmed the validity of this approach for a pair of binary MgB₂ samples but have gone on to show that it may break down for heavily doped ones. The breakdown has to do with a sample-to-sample variation of Debye temperature, θ_D . In order to take this into account we have replaced the invariant $\rho_i(T)$ with its Bloch-Grüneisen (B-G) counterpart. As a result excellent fits were obtained for the $\rho_m(T)$ s of three in-house-prepared samples as well as five published sets of $\rho_m(T)$ data, as reported elsewhere [116]. The deduced values of F for our bulk

powder-processed samples yielded connectivities of from 11 to 23%. Comparable results are expected for in-situ PIT-processed wires indicating that increases in their J_c s by factors of 4.3 – 9.1 would accompany the establishment of full connectivity.

It is important to note that F_p curves reported to date combine the effects of flux pinning and connectivity, the material's real F_p being obscured by deficient connectivity. While it is useful to compare the J_c values of various classes of superconductor (e.g., MgB₂, YBCO, and Nb₃Sn), it is essential to de-convolute the connectivity from the F_p . Doing so enables us to define the essential properties in need of improvement. Figure 14 compares the 4-K F_p s of an MgB₂ strand (actual and projected) with that of an “internal-Sn” Nb₃Sn strand. As a starting point we compare the experimental F_p for the MgB₂ (based on the I_c of the powder core divided by the internal cross-sectional area of the sheath or stabilizer) with that of the Nb₃Sn strand (based likewise on its “non-Cu J_c ”). Clearly MgB₂ cannot compete with Nb₃Sn within the liquid-He temperature range depicted here.

Next, let us for a moment assume that a well connected MgB₂ strand could be made, such that (based on the bulk-material data of Table 3) its F_p is enabled to increase by factors of 4.3 or 9.1. As illustrated in Figure 14 its 4 K F_{pmax} would increase into the range of 41 to 87 GN/m³. The latter value is comparable to the 90 GN/m³ predicted by Matsushita for a fully connected MgB₂ bulk sample based on an alternative site-percolation approach to current transport through a porous medium [10][117]. Not shown in the figure are the even greater enhancements of overall F_p that would result from: (i) increases in H_{c2} and the associated H_{irr} that would follow the addition of suitably chosen dopants especially if they were homogeneously distributed or (ii) the shift to higher fields of the position of the F_{pmax} in response to the inclusion of point pinning centers.

In displaying Figure 14, we in no way aim to minimize the difficulty of achieving the projected F_p goals, or even assert their inevitable attainment. Indeed, while we may surely expect improvements in both intrinsic and extrinsic properties, the degree to which we will be able to approach full connectivity is at present unknown. Similarly, we are constrained in the level of achievable homogeneity in H_{c2} not only by the need to dope uniformly, but also to reduce the anisotropy, or to texture the material. The main point of Figure 14 is to draw attention to the properties most in need of improvement. While flux pinning in MgB₂ is already relatively strong (comparable to that of Nb₃Sn) connectivity and doping homogeneity are the properties most in need of improvement and control.

5. Conclusion

The prospects for improving the properties of MgB₂ in wire form and rendering it suitable for numerous practical applications have been discussed from two essential standpoints, one dealing with the properties of the MgB₂ crystal or grain (the intrinsic properties) and the other having to do with ensuring that the intragranular properties are replicated in the material in strand form (the extrinsic aspect of the problem). Regarding intrinsic properties, published thin-film results indicate that the true potential of MgB₂ can be approached by the inclusion in it of carefully selected dopants that: (i) increase H_{c2} and associated H_{irr} , (ii) increase the volume pinning strength, F_p , and especially shifting its maximum to higher reduced fields by augmenting the present grain-boundary pinning with point pinning, (iii) and associate the foregoing with attention to dopant homogeneity, texturing (or, alternatively, anisotropy reduction). But in addition to the incremental improvements that are already being made to the intrinsic properties, spectacular increases in J_c (hence F_p) over all fields and temperatures will accompany reductions

in porosity and increases in connectivity. Porosity in in-situ and ex-situ-processed materials has been discussed and a new resistivity-based approach to overall connectivity measurement described. It has been estimated that full densification and the removal of intergranular blocking phases could yield across-the-board increases in J_c of up to an order of magnitude. Thus, while all of the parameters listed above are important and will continue to demand attention, the issue of most pressing urgency is connectivity enhancement.

Acknowledgements

The MgB₂ strands were supplied by HyperTech Research, Columbus, Ohio, courtesy of M. Tomsic and M. Rindfleisch. The research was supported by the U.S. Dept. of Energy, Division of High Energy Physics, under Grants No. DEFG02-95ER40900, DE-FG02-05ER84363, and DE-FG02-07ER84914.

References

- [1] J. Akimitsu, *Symposium on Transition Metal Oxides*, Sendai, Japan, 10 January 2001
- [2] C. Buzea and T. Yamashita, *Supercond. Sci. Technol.* **14** R115-R146 (2001)
- [3] C.B. Eom, M.K. Lee, J.H. Choi, *et al.*, *Nature* **411** 5580560 (2001)
- [4] V. Braccini, A. Gurevich, J.E. Giencke, *et al.*, *Phys. Rev. B* **71** 012504(4) (2005)
- [5] M. Bhatia, M.D. Sumption, and E.W. Collings, *IEEE Trans. Appl. Supercond.* **15** 3204-3206 (2005)
- [6] S.K. Chen, M. Wei, and J.L. MacManus-Driscoll, *Appl. Phys. Lett.*, **88** 192512 (2006)
- [7] J.M. Rowell, *Supercond. Sci. Technol.*, **16** R17-R27 (2003)
- [8] J.M. Rowell, S.Y. Xu, X.H. Zheng, *et al.*, *Appl. Phys. Lett.*, **83** 102-104 (2003)
- [9] D.C. Larbalestier, *et al.*, *Nature* **410** 186-189 (2001)
- [10] A. Yamamoto, J.-i. Shimoyama, K. Kishio, *et al.*, *Supercond. Sci. Technol.*, **20** 658-666 (2007)
- [11] J. Jiang, B.J. Senkowitz, D.C. Larbalestier, *et al.*, *Supercond. Sci. Technol.*, **19** L33-L36 (2006)
- [12] S.D. Bohnenstiehl *et al.*, *EUCAS-2007*, Poster entitled “MgB₂ formation via an MgB₄ route”.
- [13] V. Ferrando, P. Manfrinetti, D. Marré, *et al.*, *Phys. Rev. B* **68**, 094517(6) (2003)
- [14] P.C. Canfield and G.W. Crabtree, *Physics Today* **56** (2003)
- [15] A.Y. Liu, I.I. Mazin, and J Kortus, *Phys Rev. Lett.* **87** 087005-1 (2001)
- [16] A. Gurevich, S. Patnaik, V. Braccini, *et al.*, *Supercond. Sci. Technol.* **17** 278-286 (2004)
- [17] A. Gurevich, *Phys. Rev. B* **67** 18515(13) (2003)
- [18] A. Gurevich, *Physica C* **456** 160-169 (2007)

- [19] C. Ferdeghini, V. Ferrando, C. Tarantini, et al., *IEEE Trans. Appl. Supercond.* **15** 3234-3237 (2005)
- [20] D. Kasanathan, K.W. Lee, and W.E. Pickett, *Physica C* **424**[3-5] 116-124 (2005)
- [21] M. Angst, S.L. Bud'ko, R.H.T. Wilke, et al., *Phys. Rev. B* **71** 144512-1-6 (2005)
- [22] S.X. Dou, V. Braccini, S. Soltanian, et al., *J. Appl. Phys.* **96** (12) 7549-7555 (2004)
- [23] S. D. Bohnenstiehl, S.A. Dregia, M.D. Sumption, et al., *IEEE Trans. Appl. Supercond.* **17** (2) 2754-2756 (2007)
- [24] R.A. Ribiero, S.L. Bud'ko, C. Petrovic, et al., *Physica C* **384** 227-236 (2003)
- [25] M. Bhatia, M.D. Sumption, E.W. Collings, et al., *Appl. Phys. Lett.* **87** 042505 (3) (2005)
- [26] W.N. Kang, E. Choi et al., *Physica C* **385** 24-30 (2003)
- [27] H. Kitaguchi and T. Doi, *Supercond. Sci. Technol.* **18** 489-493 (2005)
- [28] M.P. Paranthaman, D.K. Christen et al., *Physica C* **378** 1252-1255 (2002)
- [29] A. Plecenik, P. Kus et al., *Journal of Superconductivity* **15**(6) 621-625 (2002)
- [30] M. Roussel, A.V. Pan et al., *Supercond. Sci. Technol.* **18**, 1391-1395 (2005)
- [31] J.R. Thompson, K.D. Sorge et al., *Supercond. Sci. Technol.* **18** 970-976 (2005)
- [32] S.Y. Xu, Q. Li et al., *Phys. Rev. B* **68**(224501), 1-8 (2003)
- [33] Y. Zhao, M. Ionescu et al., *Supercond. Sci. Technol.* **17** 1247-1252 (2004)
- [34] Y. Zhao, M. Ionescu et al., *IEEE Trans. Appl. Supercond.* **15**(2), 3261-3264 (2005)
- [35] Y. Zhao, M. Ionescu, et al., *Supercond. Sci. Technol.* **18**, 395-399 (2005)
- [36] K. Komori, K. Kawagishi, et al., *Appl. Phys. Lett.* **81**(6) 1047-1049 (2002)
- [37] A. Nishida, C. Taka et al., *J. Phys. Conf. Series.* **43** 293-296 (2006)
- [38] M.A. Susner, M.D. Sumption, M. Bhatia, et al., *Physica C* **456** 180-187 (2007)
- [39] V. Braccini, et al. *IEEE Trans. Appl. Supercond.* **17** (2) 2766-2769 (2007)

- [40] P. Lezza, C. Senatore, and R. Flukiger, *Supercond. Sci. Technol.* **19**(10) 1030-1033 (2006)
- [41] Z. Gao, Y. Ma, *et al.* *J. Appl. Phys.* **102**(1), 013914/1-013914/4 (2007)
- [42] S. Soltanian, J. Horvat, *et al.* *Physica C* **390**(3) 185-190 (2003)
- [43] Y. Ma, X. Zhang, A. Xu, *et al.* *Supercond. Sci. Technol* **19** **133-137** (2006)
- [44] X. Zhang, *et al.*, *Appl. Phys. Lett.* **89** 132510/1-132510/3 (2006)
- [45] C.H. Jiang, *et al.*, *Physica C* **423** 45-50 (2005)
- [46] C.H. Jiang, T. Nakane, and H. Kumakura *IEEE Trans. Appl. Supercond.* **17** 2818-2821 (2007)
- [47] C.H. Jiang, T. Nakane, and H. Kumakura, *Physica C* **436**(2) 118-122 (2006)
- [48] C.H. Jiang, T. Nakane, and H. Kumakura, *Supercond. Sci. Technol.* **18**(6) 902-906 (2005)
- [49] H. Fujii, K. Togano, and H. Kumakura, *Supercond. Sci. Technol.* **16**(4) 432-436 (2003)
- [50] S. Schlachter, B. Liu, B. W. Goldacker, *et al.*, Paper M1H02 presented at ICMC 2007
- [51] Y. Ma, H. Kumakura, *et al.* *Appl. Phys. Lett.* **83**(6) 1181-1183 (2003)
- [52] Y. Ma, H. Kumakura, *et al.*, *Supercond. Sci. Technol.* **16**(8) 852-858 (2003)
- [53] Y. Ma, H. Kumakura, *et al.*, *Physica C* **408-410** 138-139 (2004)
- [54] J. Kim, W. Yeoh, *et al.*, *Appl. Phys. Lett.* **89**(12) 122510/1-122510/3 (2006)
- [55] W. Yeoh, J. Horvat, *et al.*, *IEEE Trans. Appl. Supercond.* **17** 2929-2932 (2007)
- [56] W. Li, Y. Li, *et al.*, *Physica C* **460-462** 570-571 (2007)
- [57] Y. Zhao, Y. Yang, *et al.*, *Physica C* **463-465** 165-169 (2007)
- [58] Y. Zhao, C. Cheng, *et al.*, *Appl. Phys. Lett.* **83**(14) 2916-2918 (2003)
- [59] C. Cheng, H. Zhang, *et al.*, *Supercond. Sci. Technol.* **16**(10) 1182-1186 (2003)
- [60] A. Yamamoto, *et al.*, *IEEE Trans. Appl. Supercond.* **16**(2) 1411-1414 (2006)

- [61] A. Yamamoto, J. Shimoyama, *et al.*, *Physica C* **463-465** 807-811 (2007)
- [62] S.X. Dou, O. Shcherbakova, *et al.*, *Physical Rev. Lett.* **98**(9) 097002 (2007)
- [63] S.X. Dou, S. Soltanian, *et al.*, *Appl Phys Lett* **81**(18) 3419-3421 (2002)
- [64] A. Matsumoto, H. Kumakura, *et al.*, *Supercond. Sci. Technol.* **16**(8) 926-930 (2003)
- [65] M.D. Sumption, M. Bhatia, *et al.*, *Supercond.Sci. Technol.* **17**(10) 1180-118 (2004)
- [66] A. Yamamoto, S. Akiyasu, *et al.*, *Supercond. Sci. Technol.* **18**(10) 1323-1328 (2005)
- [67] R. Flukiger, P. Lezza, *et al.*, *IEEE Trans. Appl. Supercond.* **17** 2846-2849 (2007)
- [68] S. Ueda, *et al.*, *Supercond. Sci. Technol.* **17**(7) 926-930 (2004)
- [69] S. Chen, M. Wei, J.L. MacManus-Driscoll, *Appl. Phys.Lett.* **88**(19) 192512/1-192512/3 (2006)
- [70] C. Cheng and Y. Zhao, *Physica C* **463-465** 220-224 (2007)
- [71] I. Ansari, *et al.*, *Supercond. Sci. Technol.* **20**(8) 827-831 (2007)
- [72] H. Kishan, V.P.S. Awana, *et al.*, *Physica C* **458**(1-2) 1-5 (2007)
- [73] X.F. Pan, T. Shen, *et al.*, *Physica Status Solidi A* **204**(5) 1555-1560 (2007)
- [74] X.F. Rui, Y. Zhao, *et al.*, *Supercond. Sci. Technol.* **17**(4) 689-691 (2004)
- [75] P. Togoulev, *et al.*, *Physica C* **450**(1-2) 45-47(2006)
- [76] N. Anderson, W. Straszheim, *et al.*, *Physica C* **390**(1) 11-15 (2003)
- [77] N. Hoerhager M. Eisterer, *et al.*, *J. Phys. Conf. Ser.* **43** 500-504 (2006)
- [78] M. Mudgel, V.P.S. Awana, *et al.*, *Mod. Phys. Lett. B* **21**(14) 875-883 (2007)
- [79] S.X. Dou, S. Soltanian, *et al.*, *Supercond. Sci. Technol.* **18**(5) 710-715 (2005)
- [80] P.N. Togoulev, N.M Suleimanov and K. Conder, *Physica C* **450**(1-2) 45-47 (2006)
- [81] A. Tampieri, G. Celotti, *et al.* *Solid State Comm.* **121**(9-10) 497-500 (2002)
- [82] C. Shekhar, R. Giri, *et al.*, *J. Appl. Phys.* **101**(4), 043906/1-043906/6 (2007)

- [83] K. Shinohara, H. Ikeda, and R. Yoshizaki, *Physica C* **463-465** 471-473 (2007)
- [84] I. Kusevic E. Babic, O. Hušnjak, *et al.*, *Solid State Comm.* **132**(11) 761-765 (2004)
- [85] C. Shekhar, R. Giri, *et al.*, *Supercond. Sci. Technol.* **18**(9) 1210-1214 (2005)
- [86] S. Zhou, A. Pan, *et al.*, *Advanced Materials* **19**(10) 1373-1376 (2007), see also Y. Zhang, S.H. Zhou, A.V. Pan, *et al.*, *IEEE Trans Supercond.* **17** 2933-2936 (2007)
- [87] M.S. Al Hossain, J.H. Kim, *et al.*, *Supercond. Sci. Technol.* **20**(8) L51-L54 (2007)
- [88] C.H. Jiang, S.X. Dou, Z.X. Cheng, *et al.*, *Supercond. Sci. Technol.* **21** 065017 (2008)
- [89] X. Xu, J.H. Kim, *et al.*, *Supercond. Sci. Technol.* **19**(11) L47-L50 (2006)
- [90] M.S. Al Hossain, J.H. Kim, *et al.*, *Supercond. Sci. Technol.* **20**(1) 112-116 (2007)
- [91] H. Yamada, N. Uchiyama, *et al.*, *IEEE Trans. Appl. Supercond.* **17** 2850-2853 (2007)
- [92] D. Dew-Hughes, *Phil. Mag.* **30** 293-305 (1974)
- [93] A.M. Campbell and J.E. Evetts, *Critical Currents in Superconductors* (Taylor and Francis Ltd, London, 1972)
- [94] E.W. Collings, *Applied Superconductivity Metallurgy and Physics of Titanium Alloys*, (Plenum Press, NY, 1986) , Volume 2, Chapter 21, Part 1
- [95] Ch. Wälti, E. Felder, C. Degen, *et al.*, *Phys. Rev. B* **64** 172515(4) (2001)
- [96] S.L. Bud'ko, G. Lapertot, C. Petrovic, *et al.*, *Phys. Rev. Lett.* **86** 1877-1880 (2001)
- [97] F. Heiniger and J. Müller, *Phys. Rev.* **134** 1407-1409 (1964)
- [98] E. Bucher, F. Heiniger, and J. Müller, in *Low Temperature Physics – LT9* , J.G. Daunt *et al.*, eds (Plenum Press N.Y. 1965) pp. 482-486
- [99] E.W. Collings, *Applied Superconductivity, Metallurgy and Physics of Titanium Alloys* (Plenum Press, NY, 1986) Volume 1, pp. 390-392, 408-414
- [100] G. Giunchi, G. Ripamonti, T. Cavallin, *et al.*, *Cryogenics* **46** 237-242 (2006)

- [101] I.I. Mazin, O.K. Anderson, O. Jepsen, *et al.*, *Phys. Rev. Lett.* **89** 107002 (2002)
- [102] A.V. Sologubenko, N.D. Zhigadlo, S.M. Kazakov, *et. al.*, *Phys. Rev. B* **71** 010501-1-4 (2005)
- [103] W.L. McMillan, *Phys. Rev.* **167** 331-344 (1968)
- [104] E.W. Collings, *Applied Superconductivity, Metallurgy and Physics of Titanium Alloys* (Plenum Press, NY, 1986) Volume 1, pp. 321-322, 454-456
- [105] Y. Wang, T. Plackowski, and A. Junod, *Physica C* **355** (3-4) 179-193 (2001)
- [106] K.-P. Bohnen, R. Heid, and B. Renker, *Phys. Rev. Lett.* **86** 5771-5774 (2001)
- [107] J. Kortus, I.I. Mazin, K.D. Belaschenko, *et al.*, *Phys. Rev. Lett.* **86** 4656 (2001)
- [108] Y. Kong, O.V. Dolgov, O. Jepsen, *et al.*, *Phys. Rev. B* **64** 020501 (2001)
- [109] H.J. Choi, D. Roundy, H. Sun, *et al.*, *Phys. Rev. B* **66** 020513-1-4 (2002)
- [110] A. Brinkman, A.A. Golubov, H. Rogala, *et al.*, *Phys. Rev. B* **65** 180517-1-4 (2002)
- [111] C.-Y. Moon, Y.-H. Kim, and K.J. Chang, *Phys. Rev. B* **70** 104522-1-5 (2004)
- [112] J. Geerk, R. Schneider, G. Linker, *et al.*, *Phys. Rev. Lett.* **94** 227005-1-4 (2005)
- [113] J.M. An and W.E. Pickett, *Phys. Rev. Lett.* **86** 4366 (2001)
- [114] K.A. Yates, G. Burnell, N.A. Stelmashenko, *Phys. Rev. B* **68** 220512-1-4 (2003)
- [115] S. Tsuda, T. Yokoya, T. Kiss, *et al.*, *Phys. Rev. B* **72** 064527-1-5 (2005)
- [116] M. Bhatia, PhD Thesis, The Ohio State University, 2007.
- [117] T. Matsushita, presented at the 13th Japan-US Workshop on Advanced Superconductors, Gifu, Japan, Nov. 10-11 (2007)

List of Tables

Table 1. List of dopants added to MgB₂.

Table 2. Elemental data and molar volumes.

Table 3. Results of the BG-based resistivity analysis for binary MgB₂ and heavily doped (with TiB₂ and SiC) MgB₂ pellets.

Table 4. Estimation of an electron-phonon coupling constant based on Equation (13) and the resistively determined Debye temperature, θ_R .

Table 1. List of dopants added to MgB₂.

Nitriles borides silicides	Carbon and carbon inorganics	Metal oxides	Metallic elements	Organic compounds
Si_3N_4 ⁴⁶⁻⁴⁸ WB ⁴⁹ ZrB_2 ^{5,44} TiB_2 ⁵ NbB_2 ⁵ CaB_6 ⁵⁰ WSi_2 ^{51,52,53} $ZrSi_2$ ^{51,52}	C nanotubes ⁵⁴⁻⁵⁷ $Nanodiamond$ ⁵⁷⁻⁵⁹ TiC ^{60,61} SiC ^{38,42,62-65} B_4C ^{40,66,67} Na_2CO_3 ⁶⁸	Dy_2O_3 ⁶⁹ HoO_2 ⁷⁰ Al_2O_3 ⁷¹ MgO ⁴⁵ TiO_2 ⁷² Pr_6O_{11} ⁷³ SiO_2 ⁷⁴	Ti ⁷⁵⁻⁷⁷ Zr ⁷⁷ Mo ⁷⁸ Fe ⁷⁹ Co ⁸⁰ Ni ⁸⁰ Cu ⁸¹ Ag ⁸² Al ⁸³ Si ⁸⁴ La ⁸⁵	$Sugar$ ⁸⁶ $malic\ acid$ ⁸⁷ $maleic\ anhydride$ ⁴¹ $paraffin$ ⁸⁸ $toluene$ ⁸⁹ $ethanol$ ⁸⁹ $acetone$ ⁸⁹ $tartaric\ acid$ ⁹⁰ $ethyltoluene$ ⁹¹

Table 2. Elemental data and molar volumes.

Element	Density ρ , g/cc	At/molar wgts, g	Wgts per mol MgB ₂ , g	Vols per mol MgB ₂ , cc
Mg	1.77	24.32	24.32	13.74
B	2.34	10.82	21.64	9.25
MgB ₂	2.67	45.96	45.96	17.21

Table 3. Results of the BG-based resistivity analysis for binary MgB₂ and heavily doped (with TiB₂ and SiC) MgB₂ pellets.

Sample	$\rho_0, \Omega\text{cm}$	θ_R, K	F	% Connectivity $100/F$
MB700 (binary)	11.29	677	4.32	23
MBTi800 (TiB ₂)	9.49	764	9.50	11
MBSiC700 (SiC)	38.56	593	7.39	14

Table 4. Estimation of an electron-phonon coupling constant based on Equation (13) and the resistively determined Debye temperature, θ_R .

Sample	Onset T_c , K	θ_R , K	θ_D , K	λ ($\mu^*=0.10$)
MB700 (binary)	38.0	677	653	0.98
MBTi800 (TiB ₂)	36.5	764	745	0.89
MBSiC700 (SiC)	35.5	593	600	1.02

List of Figures

- Fig. 1. Resistively measured upper critical fields of eight MgB₂ films, after Ferdeghini *et al.* [19].
- Fig. 2. DSC traces showing the decomposition of SiC near 524°C and the onset of MgB₂ formation near 615°C. Solid line is Mg only (Mg melting at 650°C), Dash-dot line is mixed Mg and B (complete MgB₂ below Mg melting), and dashed line is SiC+ Mg powders (reduction of SiC by Mg at 524°C).
- Fig. 3. Increases in the irreversibility field of MgB₂ in response to doping with 7.5 mol% ZrB₂.
- Fig. 4. 4 K Transport J_{cs} of MgB₂ films made by various techniques including e-beam evaporation, thermal co-evaporation, hybrid physical-chemical vapor deposition, and pulsed-laser deposition (PLD), both in-situ and ex-situ.
- Fig. 5. The J_{cs} of some early commercially produced binary MgB₂ wires compared to selected thin film results.
- Fig. 6. Enhancements in strand-based transport J_c obtained by (i) increasing the Mg content and (ii) doping the result with fine SiC particles.
- Fig. 7. A comparison of thin film results to recent measurements on MgB₂ strands with various dopants.
- Fig. 8. Normalized bulk pinning force curves for sample of an MgB₂ strand doped with 5% SiC (particle size 30 nm).
- Fig. 9a. Total low temperature specific heat of MgB₂ with 5 mol% SiC and 7.5 mol% TiB₂ compared to that of a binary, control MgB₂.

- Fig. 9b. Electronic specific heat of MgB_2 with SiC and TiB_2 additions, as compared to a binary control MgB_2 .
- Fig. 10. SEM micrograph of an $\text{Mg}_{1.15}\text{B}_2$ monocore PIT strand after 40min/700°C.
- Fig. 11. Packing density of MgB_2 formed from equi-sized Mg and B particles, Model-(1), and that formed from large Mg particles imbedded in fine B powder, Model-(2)
- Fig. 12. Schematic illustration of the combined presence of pores and intergranular film showing general porosity or general lack of connectivity.
- Fig. 13. Measured resistivity temperature dependence, $\rho_m(T)$, for binary and doped MgB_2 samples.
- Fig. 14. Field dependence of bulk pinning force density, F_p , for present day MgB_2 strand, and estimated strand results assuming 4x and 9x greater connectivity. Results are compared to present day HEP class Nb_3Sn conductor.

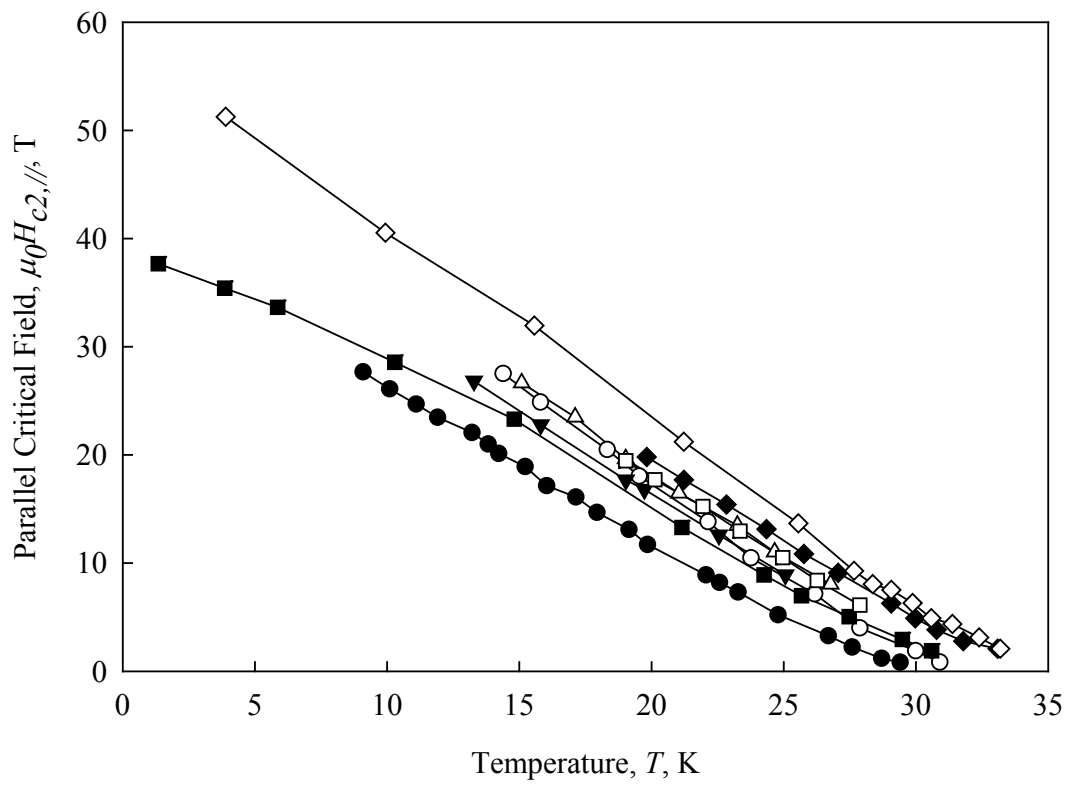


Figure 1.

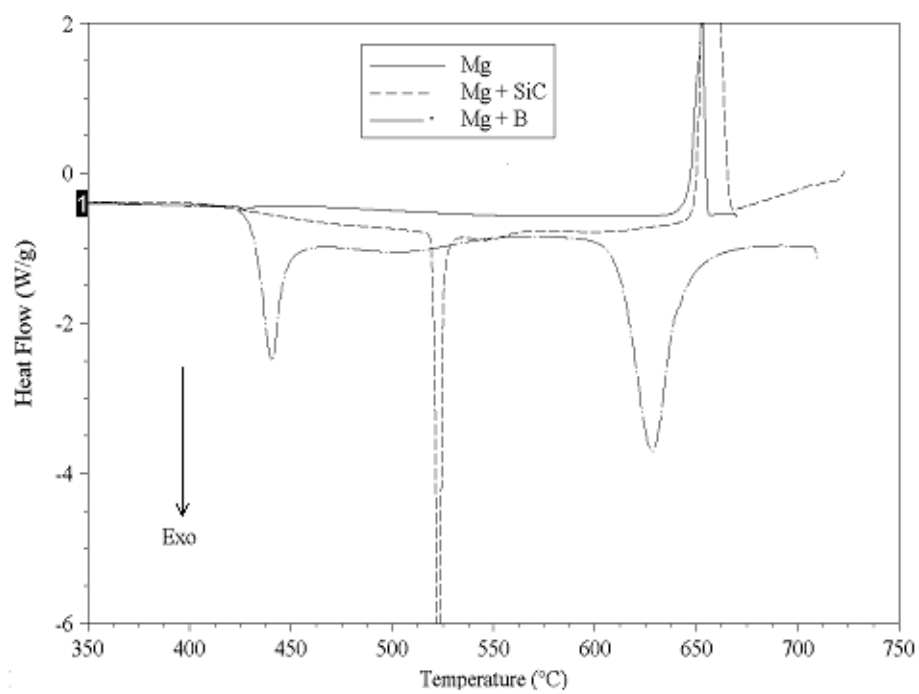


Figure 2.

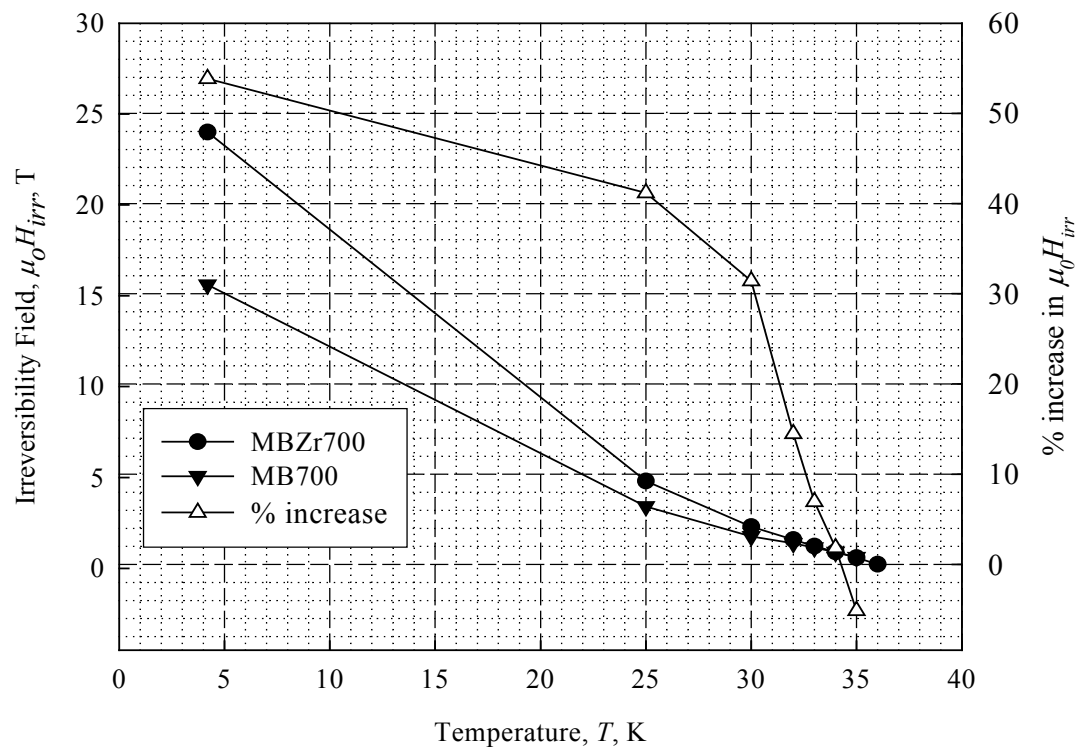


Figure 3.

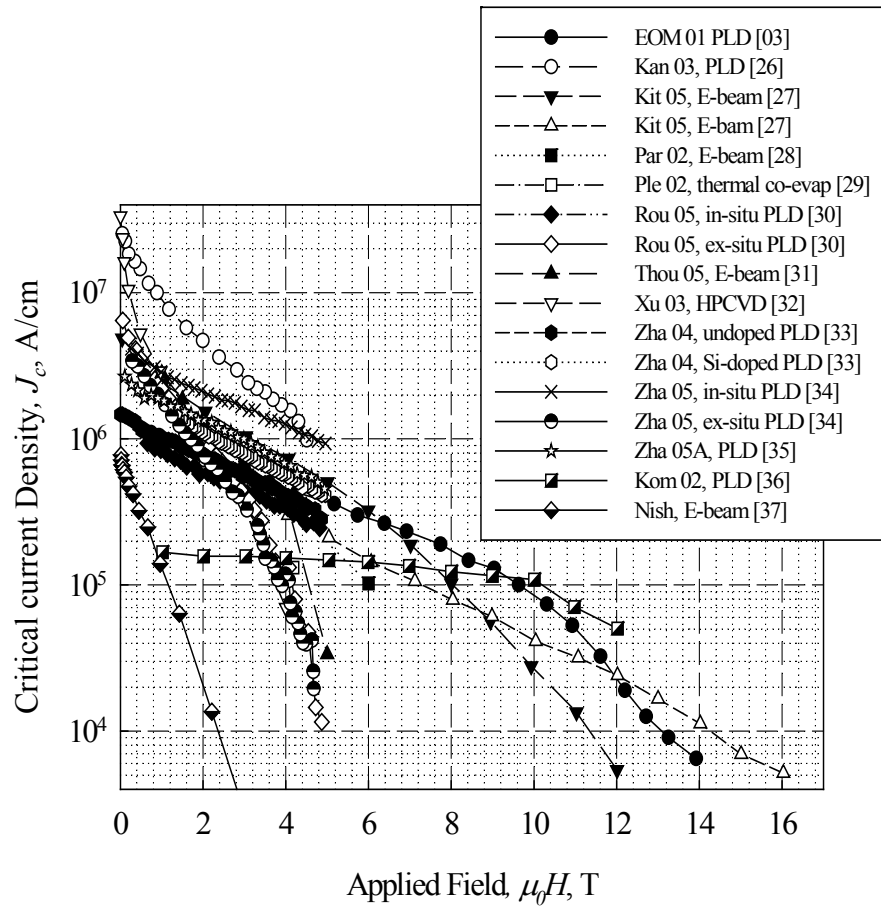


Figure 4.

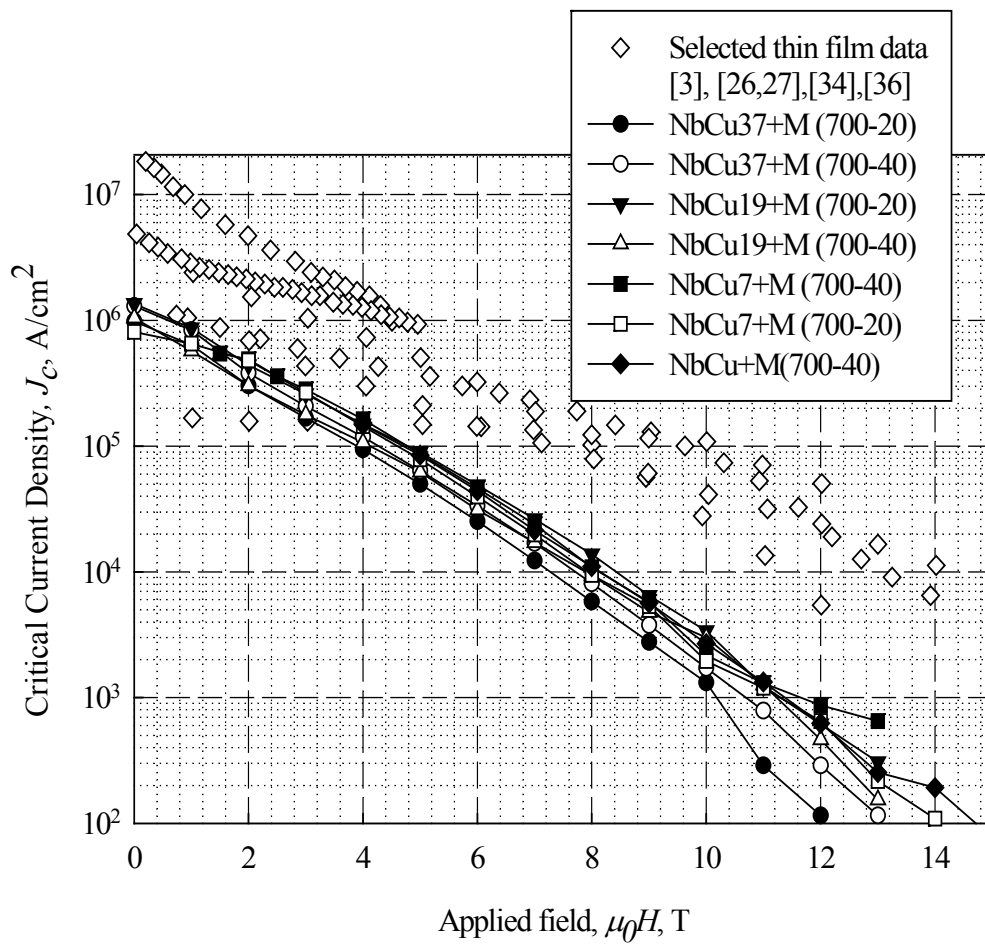


Figure 5.

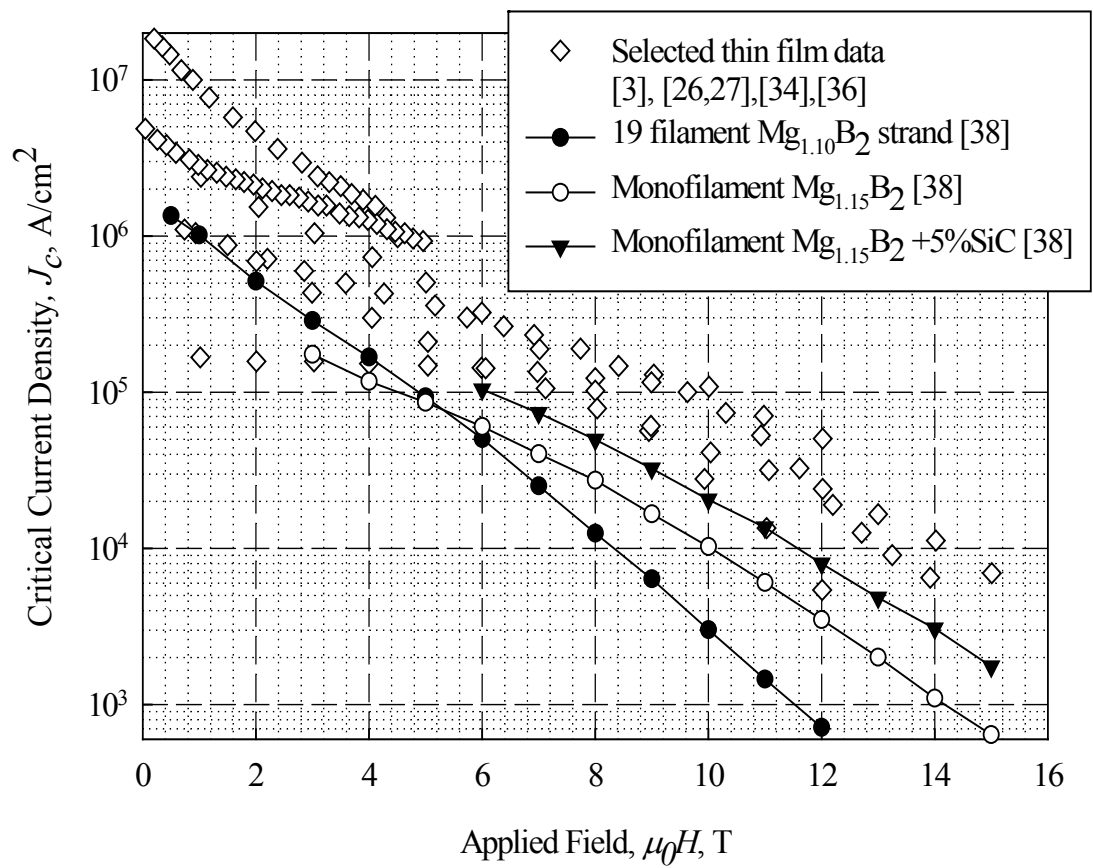


Figure 6.

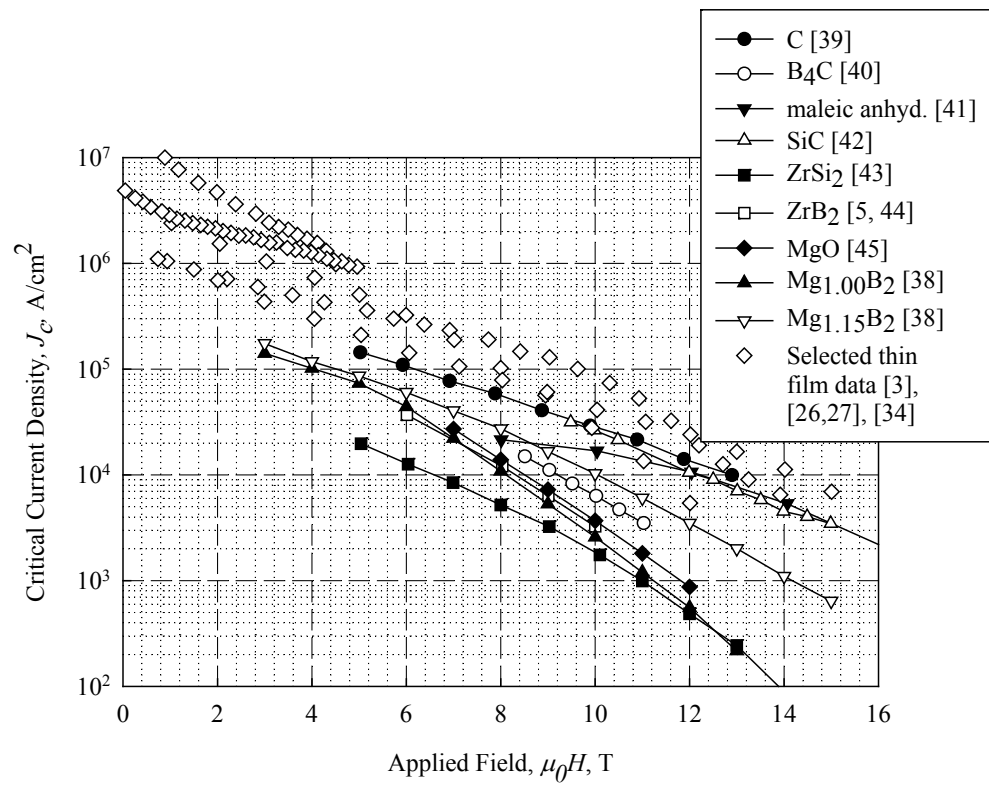


Figure 7.

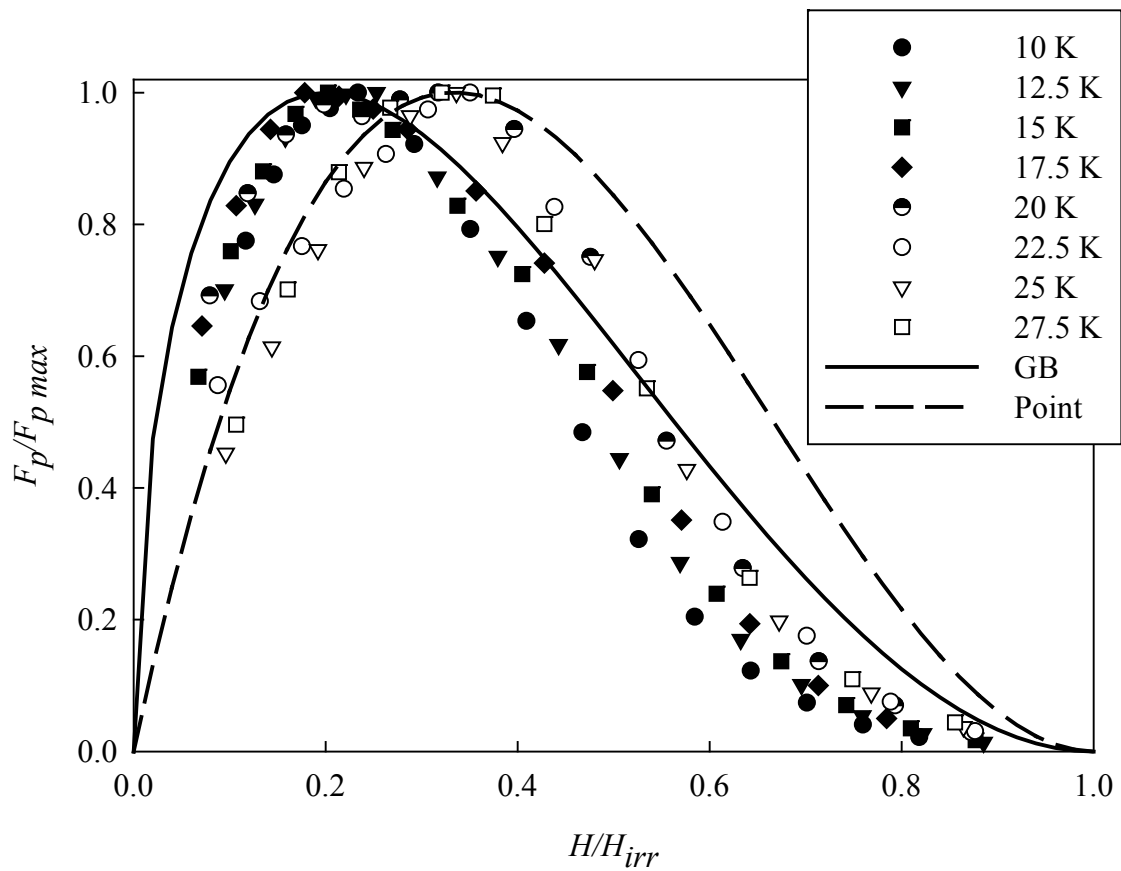


Figure 8.

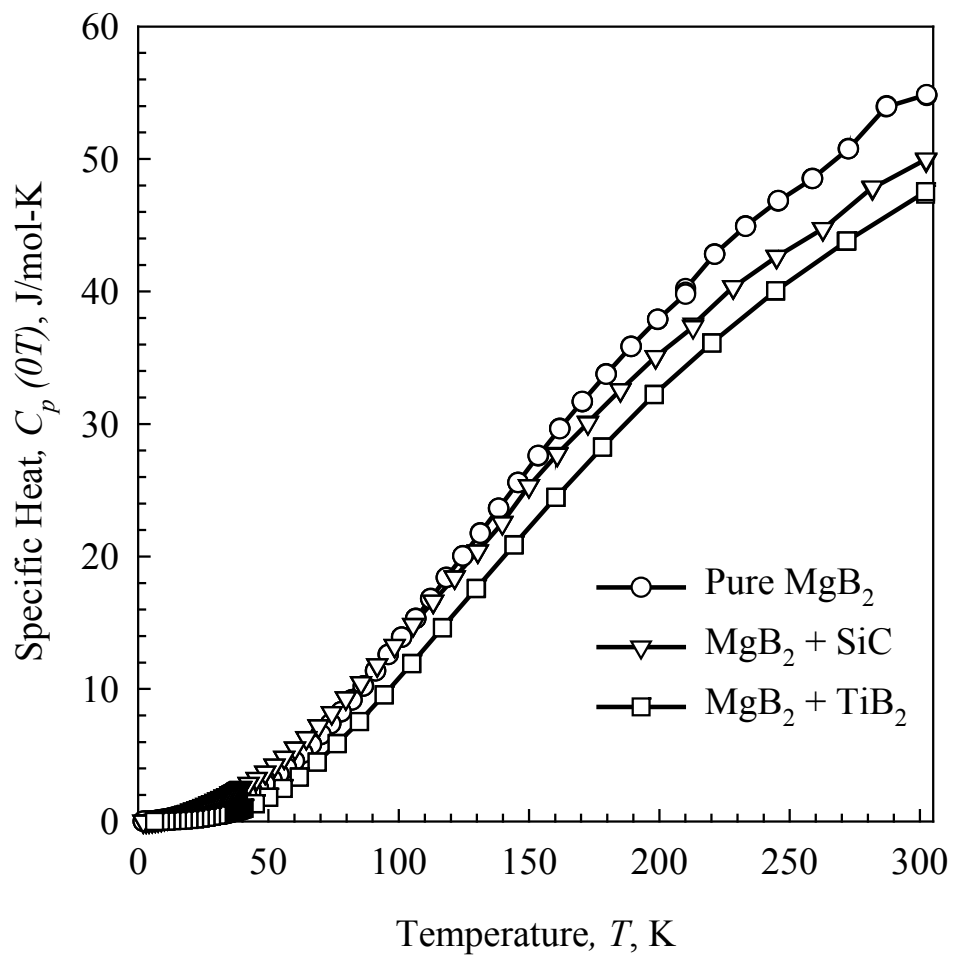


Figure 9a.

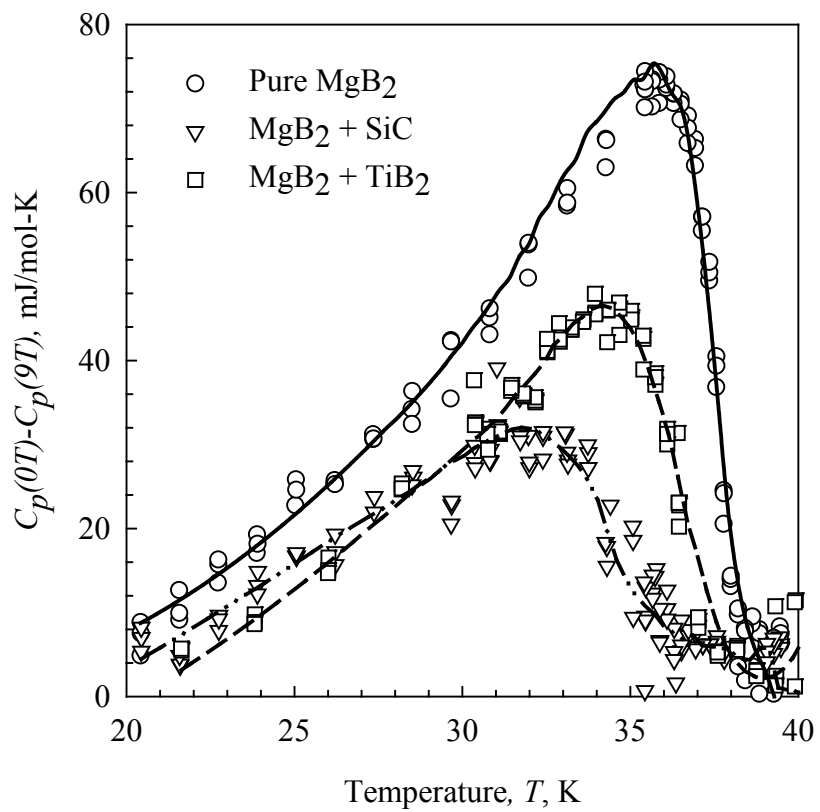


Figure 9b.

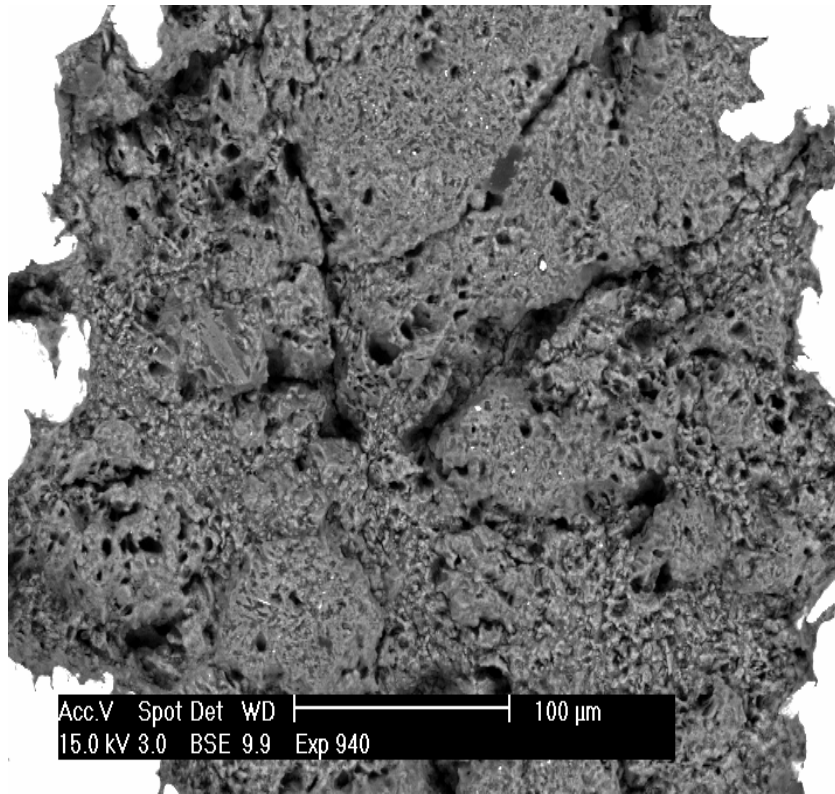


Figure 10.

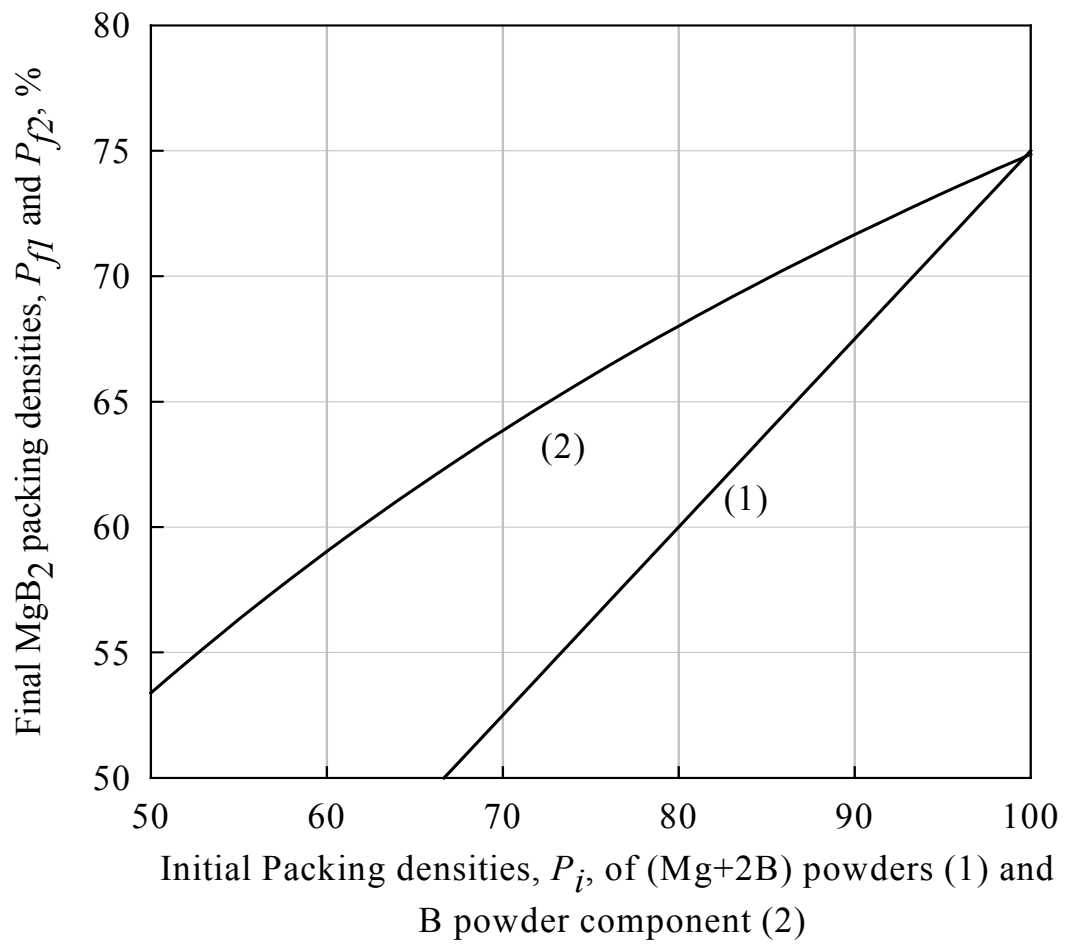


Figure 11.

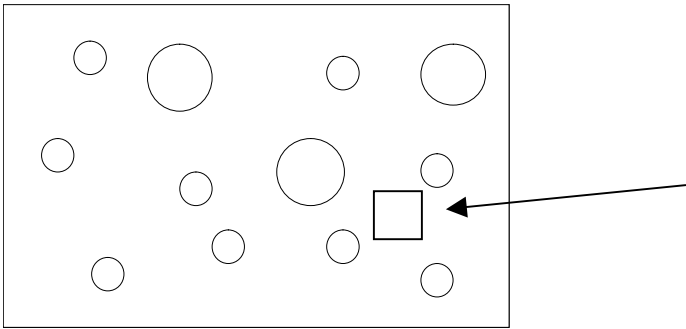


Figure 12.

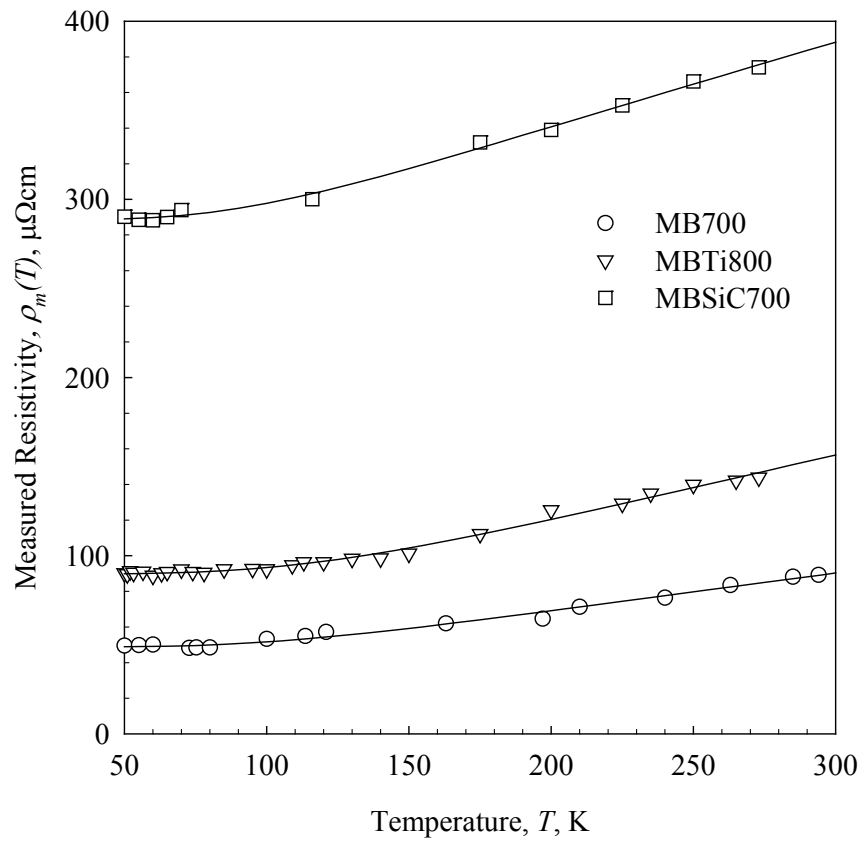


Figure 13.

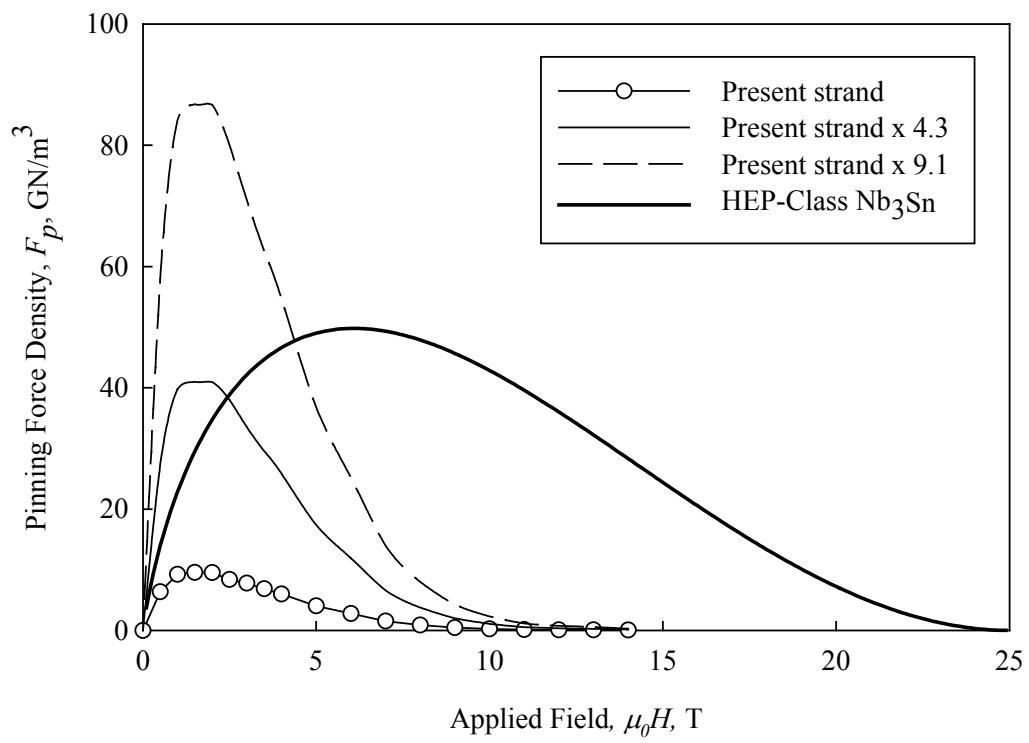


Figure 14